DOI 10.1007/s11182-016-0855-z

Russian Physics Journal, Vol. 59, No. 7, November, 2016 (Russian Original No. 7, July, 2016)

PHYSICS OF SEMICONDUCTORS AND DIELECTRICS

TEMPERATURE AND FIELD DEPENDENCES OF PARAMETERS OF THE EQUIVALENT CIRCUIT ELEMENTS OF MIS STRUCTURES BASED ON MBE *n*-$Hg_{0.775}Cd_{0.225}Te$ IN THE STRONG INVERSION MODE

A. V. Voitsekhovskii,[1,2] S. N. Nesmelov,[1,2] and S. M. Dzyadukh[1,2]

UDC 621.315.592

A technique is proposed for the determining the parameters of the equivalent circuit elements in strong inversion mode using the measurement results of the admittance of MIS structures based on n-$Hg_{0.775}Cd_{0.225}Te$ *grown by molecular beam epitaxy. It is shown that at 77 K and frequencies above 10 kHz, the capacitance-voltage characteristics of MIS structures based on n-*$Hg_{0.775}Cd_{0.225}Te$ *with a near-surface graded gap layer have a high-frequency behavior with respect to the recharge time of surface states located near the Fermi level of intrinsic semiconductor. It is established that the electron concentration in the near-surface graded-gap layer exceeds an average concentration found by the Hall method by more than 2 times. The proposed technique was used for determining the temperature dependences of the insulator capacitance, capacitance and differential resistance of the space-charge region, and capacitance of the inversion layer in MIS structures based on n-*$Hg_{0.775}Cd_{0.225}Te$ *without a graded-gap layer. The temperature and voltage dependences of the parameters of the equivalent circuit elements in strong inversion are calculated. The results of calculation are qualitatively consistent with the results obtained from the measurements of the admittance.*

Keywords: a MIS structure, HgCdTe, molecular beam epitaxy, a graded-gap layer, capacitance-voltage characteristic, capacitance and resistance of the space-charge region, capacitance of the inversion layer.

INTRODUCTION

Selection of an optimal passivation coating is an important practical problem in the development of highly sensitive infrared detectors based on the semiconductor $Hg_{1-x}Cd_xTe$ solid solution [1, 2]. To assess the quality of passivating insulator layers, electrical characteristics of MIS structures are often studied [3–6]. Research methods designed for silicon MOS-structures [7] are not suitable in an unchanged form for studying MIS structures based on $Hg_{1-x}Cd_xTe$ grown by molecular beam epitaxy (MBE), which is associated not only with the fundamental differences in properties of semiconductor materials. A peculiarity of MIS structures based on MBE HgCdTe is a noticeable effect of the resistance of the epitaxial film bulk on the measured capacitance and conductance, which usually occurs at frequencies above 100 kHz [8]. Another peculiarity is the presence in the epitaxial HgCdTe films of graded-band near-surface layers with high content of CdTe, which are grown in order to reduce the influence of surface recombination on the lifetime in the bulk of semiconductor [9]. In this regard, experimental and theoretical studies of mechanisms of formation of electrical and photoelectric characteristics of MIS structures based on MBE HgCdTe appear relevant.

[1]National Research Tomsk State University, Tomsk, Russia, e-mail: vav43@mail.tsu.ru; nesm69@mail.ru; bonespirit@mail2000.ru; [2]V. D. Kuznetsov Siberian Physical-Technical Institute at Tomsk State University, Tomsk, Russia, Translated from Izvestiya Vysshikh Uchebnykh Zavedenii, Fizika, No. 7, pp. 8–18, July, 2016. Original article submitted April 19, 2015.

Some peculiarities of electrophysical and photoelectric characteristics of MIS structures based on MBE HgCdTe are described in [10–17]. However, determining the majority charge carrier concentration in the near-surface layer of HgCdTe using electrical measurements has long been an unsolved problem. Earlier, temperature and voltage dependences of the differential resistance of the space charge region (SCR) have been investigated on the basis of measurements of the frequency dependences of the conductance in MIS structures based on MBE *p*-$Hg_{0.78}Cd_{0.22}Te$ [16]. Recently, a technique has been proposed that allows finding the capacitance and resistance of the SCR and the capacitance of the inversion layer from the measurements of the admittance of MIS structures based on MBE *p*-$Hg_{0.78}Cd_{0.22}Te$ at intermediate frequencies of the AC test signal (50 kHz - 1 MHz). It was shown that at frequencies of 50 kHz, the capacitance-voltage characteristics (CV characteristics) of MIS structures based on MBE *p*-$Hg_{0.78}Cd_{0.22}Te$ with a graded-gap layer have a high-frequency behavior with respect to the recharge time of surface states, while the CV characteristics of MIS structures based on *p*-$Hg_{0.78}Cd_{0.22}Te$ of uniform composition at 50 kHz are not high-frequency with respect to the recharge time of surface states. Determining the parameters of elements of the equivalent circuit in strong inversion for MIS structures based on MBE *n*-$Hg_{1-x}Cd_xTe$ (x = 0.21–0.23) meets additional difficulties due to the effects of degeneracy and nonparabolicity of the conduction band [3, 18-21], which underestimate the capacitance values in the accumulation mode and cause a need to develop a method of finding the insulator capacitance.

The aim of this work is to study the peculiarities of definition of parameters of the equivalent circuit elements in strong inversion using the measurements of the admittance of MIS structures based on MBE *n*-$Hg_{0.775}Cd_{0.225}Te$ to develop a technique for determining the dopant concentration in the near-surface layer of the semiconductor and to study the temperature and voltage dependences of the parameters of the equivalent circuit elements in the strong inversion mode for MIS structures based on MBE *n*-$Hg_{0.775}Cd_{0.225}Te$.

SAMPLES AND EXPERIMENTAL PROCEDURES

The MIS structures under study were fabricated on the basis of *n*-$Hg_{0.775}Cd_{0.225}Te$ grown by MBE on the substrates of GaAs (013). When growing a heterostructure, graded-band layers with high component composition of CdTe were created on both sides of the working layer. Prior to the deposition of insulator coatings, electron concentration ($4.7\cdot10^{14}$ cm^{-3}), electron mobility (88000 $cm^2\cdot V^{-1}\cdot s^{-1}$), and the conductivity (6.8 $\Omega^{-1}\cdot cm^{-1}$) were determined in the heterostructure under study at 78 K by the Hall method. The lifetime at 77 K found by a contactless microwave method was 3.6–4.0 μs.

For the structure No. 1, the near-surface graded-gap layer was previously removed by etching the surface in the Br_2–HBr solution and then, an insulator coating – aluminum oxide Al_2O_3 – was formed by plasma enhanced atomic-layer deposition (PE ALD) [22]. The structure No. 2 had a near-surface graded-gap layer with high content of CdTe (the composition on the surface of 0.43, the thickness of the upper graded-gap layer of 0.5 μm, and the thickness of the working layer of 8.6 μm). For the structure No. 2, a double-layer insulator SiO_2/Si_3N_4 was deposited as the insulator coating [23]. The indium electrode area was $1.762\cdot10^{-7}$ m^2 for the structure No. 1 and $3.079\cdot10^{-7}$ m^2 for the structure No. 2. In the calculations, to approximate the distribution of the composition x over the coordinate z in the near-surface layer of the structure No. 2, the following formula was used:

$$x(z) = x_0 + A_1 \cdot \exp\left(-\frac{z}{B_1}\right),$$

where x_0 = 0.22221, A_1 = 0.21689, and $B_1 = 1.7356\cdot10^{-7}$ m.

The measurements were performed with an automated setup of the admittance spectroscopy of nanoheterostructures on the basis of a non-optical cryostat Janis and immittance meter Agilent E4980A. In the measurements, as the forward and reverse directions of sweep, the voltage change from the negative values to the positive ones and that from the positive values to the negative ones were taken, respectively.

In the measurements, a parallel equivalent circuit was used, i.e., the resistance (R_{meas}) and capacitance (C_{meas}) of the MIS structure were measured at their parallel connection, as shown in Fig. 1*a*. To determine the capacitance of the insulator C_{ins} and the resistance of the epitaxial film bulk (R_s) characterizing the working layer, the values of the

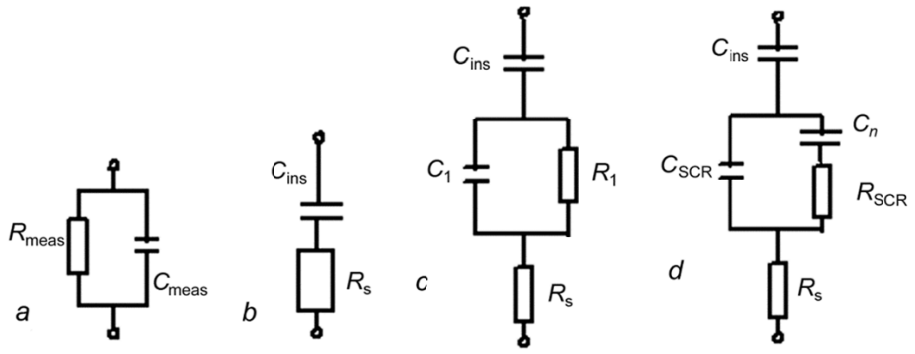

Fig. 1. Parallel equivalent circuit (*a*) and equivalent circuits of MIS structures in the accumulation (*b*) and inversion (*c*, *d*) modes.

capacitance and the resistance of the MIS-structure in the accumulation mode, when the equivalent circuit of Fig. 1*b* is correct, were used.

The bulk resistance is determined mainly by geometrical parameters of the homogeneous working layer of the epitaxial film between the back contact and metal field electrode, as well as by the initial conductance of the epitaxial film material (the working layer). The insulator capacitance and the bulk resistance were calculated using the following formulas [8, 13]:

$$R_s = \frac{R_{meas}}{1+\omega^2 C_{meas}^2 R_{meas}^2},\ C_{ins} = \frac{1+\omega^2 C_{meas}^2 R_{meas}^2}{\omega^2 C_{meas} R_{meas}^2}. \tag{1}$$

In the depletion and inversion modes, electric field of the space charge region (SCR) can penetrate deep into the epitaxial film to a distance equal to the SCR width in the strong inversion mode. The capacitance (C_1) and the resistance (R_1) of this near-surface semiconductor layer (the equivalent circuit in Fig. 1*c*) can be determined using the expressions given in [8, 13]:

$$R_1 = \frac{1-\omega^2 C_{meas} R_{meas}^2 \left(2C_{ins} - C_{meas}\right) + \omega^2 C_{ins}^2 \left(R_{meas}\left(R_{meas} - 2R_s\right) + R_s^2\left(1+\omega^2 C_{meas}^2 R_{meas}^2\right)\right)}{\omega^2 C_{ins}^2 \left(R_{meas} - R_s - \omega^2 C_{meas}^2 R_s R_{meas}^2\right)}, \tag{2}$$

$$C_1 = \frac{C_{ins}\left(\omega^2 (C_{ins} - C_{meas}) C_{meas} R_{meas}^2 - 1\right)}{1-\omega^2 C_{meas} R_{meas}^2 \left(2C_{ins} - C_{meas}\right) + \omega^2 C_{ins}^2 \left(R_{meas}\left(R_{meas} - 2R_s\right) + R_s^2\left(1+\omega^2 C_{meas}^2 R_{meas}^2\right)\right)}. \tag{3}$$

In the inversion mode, the equivalent circuit of the MIS structure takes a form shown in Fig. 1*d* [6, 24]. We can calculate the capacitance and resistance of the near-surface layer of the semiconductor by the formulas

$$R_1 = \frac{1+\omega^2 C_p^2 R_{SCR}^2}{\omega^2 C_p^2 R_{SCR}},\ C_1 = C_{SCR} + \frac{C_p}{1+\omega^2 C_p^2 R_{SCR}^2}. \tag{4}$$

In so doing, $\tau_i = R_{SCR} \cdot C_p$ is the relaxation time of the inversion layer capacitance, R_{SCR} is the differential resistance of the SCR, C_{SCR} is the SCR capacitance (the capacitance of the depletion layer), C_p is the capacitance of the inversion layer.

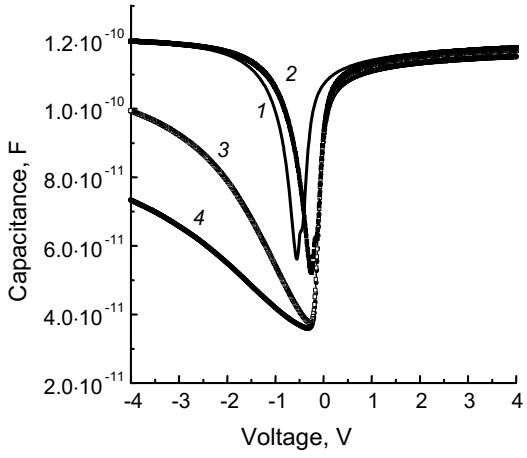

Fig. 2

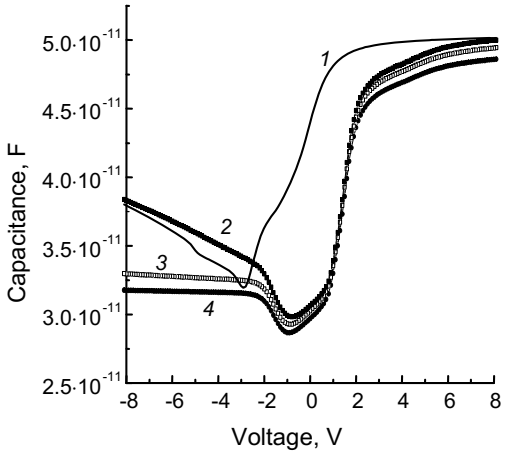

Fig. 3

Fig. 2. CV characteristics of the MIS structure based on *n*-HgCdTe without a graded-gap layer (the structure No. 1) measured at a temperature of 77 K under the forward (*1*) and reverse (*2–4*) voltage sweeps at frequencies, kHz: 100 (*1*, *2*), 500 (*3*), and 1000 (*4*).

Fig. 3. CV characteristics of the MIS structure based on *n*-HgCdTe with a graded-gap layer (the structure No. 2) measured at a temperature of 77 K under the forward (*1*) and reverse (*2–4*) voltage sweeps at frequencies, kHz: 100 (*1*, *2*), 500 (*3*), and 1000 (*4*).

EXPERIMENTAL RESULTS AND DISCUSSION

Figures 2 and 3 show the CV characteristics of MIS structures Nos. 1 and 2, respectively, measured at a temperature of 77 K at different frequencies under the forward and reverse voltage sweeps. The effect of the bulk resistance of the epitaxial film on the measured capacitance is excluded for both structures [8, 13].

Figures 2 and 3 demonstrate that for the MIS-structure No. 1 with the Al_2O_3 insulator, the capacitance of the MIS structure in the accumulation mode is 2.5 times higher, than for the structure No. 2 with a double-layer insulator SiO_2/Si_3N_4. This is due to the differences in the thicknesses and permittivities of different passivating coatings. The CV characteristics of the structure No. 2 have a more pronounced high-frequency behavior, if we compare the dependences at the same frequency (for example, at 100 kHz). For the CV characteristics of the structure No. 1, the value of the capacitance in the minimum depends on the frequency. Practically no such dependence is observed for the structure No. 2 with a graded-gap layer. For the structure No. 1 without a graded-gap layer, hysteresis of CV characteristics and the plane wave voltage are smaller. The capacitance value at the minimum of the CV characteristic measured at a frequency of 100 kHz is higher at the direct voltage sweep for both structures.

Figures 4 and 5 show the CV characteristics of MIS structures No. 1 and No. 2, respectively, measured at a temperature of 10 K at different frequencies under the forward and reverse voltage sweeps. It is seen from Figs. 4 and 5 that for the structure No. 1, cooling led to a low-frequency behavior of the CV-characteristics and for the structure No. 2, it resulted in a high-frequency behavior. There is practically no frequency dependence of the capacitance value in the minimum of the CV-characteristics at 10 K for the structure No. 1. For the structure No. 2, hysteresis of the CV-characteristics is decreased markedly while cooling. Causes of the low temperature maxima of the capacitance in the inversion for the structure No. 2 remain debatable. The capacitance minima are accompanied by the appearance of the conductance maxima, which is characteristic for the surface levels [7]. However, the frequency and temperature dependences of the capacitance and conductance at the maxima are not typical for the surface levels.

To determine the parameters of the equivalent circuit elements (C_{ins}, C_p, R_{SCR}, C_{SCR}), the values of the capacitance C_{meas} and resistance $R_{meas} = 1/G_{meas}$ were measured at two frequencies $f_1 = \omega_1/2\pi$ and $f_2 = \omega_2/2\pi$

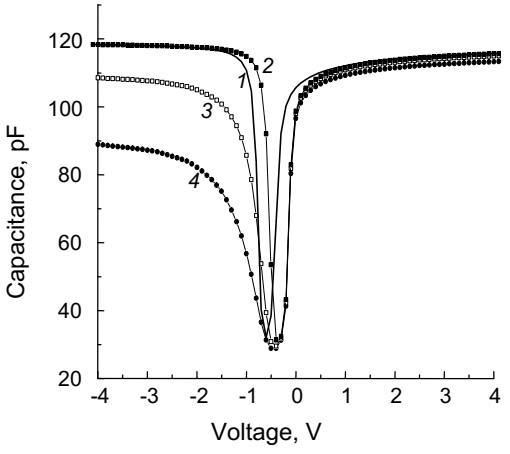

Fig. 4

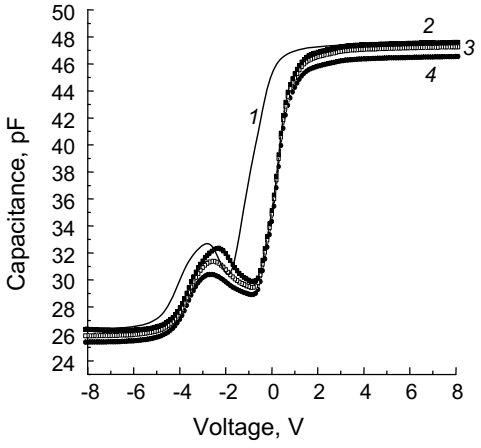

Fig. 5

Fig. 4. CV characteristics of the MIS structure based on *n*-HgCdTe without a graded-gap layer (the structure No. 1) measured at a temperature of 10 K under the forward (*1*) and reverse (*2–4*) voltage sweeps at frequencies, kHz: 100 (*1*, *2*), 500 (*3*), and 1000 (*4*).

Fig. 5. CV characteristics of the MIS structure based on *n*-HgCdTe with a graded-gap layer (the structure No. 2) measured at a temperature of 10 K under the forward (*1*) and reverse (*2–4*) voltage sweeps at frequencies, kHz: 100 (*1*, *2*), 500 (*3*), and 1000 (*4*).

($C_{meas1} = C_{meas}(f_1)$, $R_{meas1} = R_{meas}(f_1)$, $C_{meas2} = C_{meas}(f_2)$, $R_{meas2} = R_{meas}(f_2)$, respectively). The frequencies f_1 and f_2 must comply with the intermediate behavior of the CV characteristics. At each frequency, the resistances $R_{s1} = R_s(f_2)$ and $R_{s2} = R_s(f_2)$ of the epitaxial film bulk were determined using the formula (1). Here, the frequency dependence of the insulator capacitance was taken into account, assuming that the insulator capacitance depends on the frequency in a similar way as the MIS-structure capacitance in the accumulation mode ($C_{acc} = C_{acc}(f)$) after eliminating the effect of the bulk resistance ($k_2 = C_{acc2}(f_2)/C_{acc1}(f_1)$). As a result, a system of four equations was constructed:

$$\frac{1-\omega_1^2 C_{meas1} R_{meas1}^2 \left(2C_{ins} - C_{meas1}\right) + \omega_1^2 C_{ins}^2 \left(R_{meas1}\left(R_{meas1} - 2R_{s1}\right) + R_{s1}^2\left(1+\omega_1^2 C_{meas1}^2 R_{meas1}^2\right)\right)}{\omega_1^2 C_{ins}^2 \left(R_{meas1} - R_{s1} - \omega_1^2 C_{meas1}^2 R_{s1} R_{meas1}^2\right)} = \frac{1+\omega_1^2 C_p^2 R_{SCR}^2}{\omega_1^2 C_p^2 R_{SCR}},$$

$$\frac{C_{ins}\left(\omega_1^2 (C_{ins} - C_{meas1}) C_{meas1} R_{meas1}^2 - 1\right)}{1-\omega_1^2 C_{meas1} R_{meas1}^2 \left(2C_{ins} - C_{meas1}\right) + \omega_1^2 C_{ins}^2 \left(R_{meas1}\left(R_{meas1} - 2R_{s1}\right) + R_{s1}^2\left(1+\omega_1^2 C_{meas1}^2 R_{meas1}^2\right)\right)}, \quad (5)$$

$$= C_{SCR} + \frac{C_p}{1+\omega_1^2 C_p^2 R_{SCR}^2}$$

$$\frac{1-\omega_2^2 C_{meas2} R_{meas2}^2 \left(2k_2 C_{ins} - C_{meas2}\right) + \omega_2^2 k_2^2 C_{ins}^2 \left(R_{meas2}\left(R_{meas2} - 2R_{s2}\right) + R_{s2}^2\left(1+\omega_2^2 C_{meas2}^2 R_{meas2}^2\right)\right)}{\omega_2^2 k_2^2 C_{ins}^2 \left(R_{meas2} - R_{s2} - \omega_2^2 C_{meas2}^2 R_{s2} R_{meas2}^2\right)} = \frac{1+\omega_2^2 C_p^2 R_{SCR}^2}{\omega_2^2 C_p^2 R_{SCR}},$$

TABLE 1. Values of the Equivalent Circuit Elements for the Structures Nos. 1 and 2 Determined at 77 K

Number of the structure	C_{ins}, pF	R_{SCR}, Ω	C_p, pF	C_{SCR}, pF
1	129.9	872	1860	60.5
2	55.2	17358	975	66.9

$$\frac{k_2 C_{ins}\left(\omega_2^2(k_2 C_{ins} - C_{meas2})C_{meas2}R_{meas2}^2 - 1\right)}{1 - \omega_2^2 C_{meas2}R_{meas2}^2\left(2k_2 C_{ins} - C_{meas2}\right) + \omega_2^2 k_2^2 C_{ins}^2\left(R_{meas2}\left(R_{meas2} - 2R_{s2}\right) + R_{s2}^2\left(1 + \omega_2^2 C_{meas2}^2 R_{meas2}^2\right)\right)} = C_{SCR} + \frac{C_p}{1 + \omega_2^2 C_p^2 R_{SCR}^2}.$$

The system was solved numerically with respect to the elements of the equivalent circuit by the secant method. In using this method, it is especially important to select the first two approximations for each of the variables. Table 1 shows the equivalent circuit element values determined at 77 K according to the proposed method for MIS-structures based on *n*-$Hg_{0.775}Cd_{0.225}Te$ without a graded-gap layer (the structure No. 1, f_1 = 200 kHz and f_2 = 500 kHz) and with a graded-gap layer (the structure No. 2, f_1 = 50 kHz and f_2 = 200 kHz).

Knowing the values of C_{ins} and C_{SCR}, it is easy to calculate the value of the high-frequency MIS-structure capacitance in the strong inversion mode by formula $C_{HFinv} = \frac{C_{ins} \cdot C_{SCR}}{C_{ins} + C_{SCR}}$, because with increasing frequency ω, the capacitance C_1 of the near-surface layer of the semiconductor tends to C_{SCR}. The dopant concentration can be found numerically by calculating an ideal high-frequency CV characteristic, for which the capacitance in the strong inversion mode will coincide with the value found from the experimental data (C_{HFinv}). The ideal CV characteristics were calculated by numerical solution of the Poisson equation with taking into account the real distribution of the composition over the coordinate at various concentrations of donor-type defects [25]. Low-frequency CV characteristics were also calculated at different concentrations of dopant, so that the calculated capacitance in the minimum coincided with the experimental value determined at a frequency of 100 kHz (C_{LFmin}). Table 2 shows the values of C_{HFinv} and C_{LFmin} for the structures Nos. 1 and 2, as well as the concentrations of dopant determined from the values C_{HFinv} and C_{LFmin}. Table 2 also shows the value of the dopant concentration determined from the slope of the dependence $1/C^2(V)$ in the depletion mode [26, 27].

Table 1 demonstrates unexpectedly large values of the insulator capacitance and unexpectedly low values of the capacitance of the inversion layer. It should be noted that the capacitance of the inversion layer for the structure No. 1 without a graded-gap layer is substantially greater than that for the structure No. 2 with a graded-gap layer, which may be associated with a lower concentration of minority carriers at a given bias voltage for the structure with a graded-gap layer, where the intrinsic concentration is lower. The resistance of SCR for the structure without a graded-gap layer is considerably less than that for the structure with a graded-gap layer, which is a consequence of the increase of the band gap width in the near-surface layer of the semiconductor for the structure No. 2 with a graded-gap layer. It follows from Table 2 that the concentration determined by the proposed method is close enough to the concentration determined from the value of the capacitance at the minimum of the low-frequency CV-characteristic for the structure No. 2 with a graded-gap layer. This suggests that for the structure with a graded-gap layer, surface states located near the Fermi level of intrinsic semiconductor do not have time to recharge when changing alternating test voltage at a frequency of 100 kHz. At 100 kHz, CV characteristics of the MIS-structure No. 2 have a high-frequency behavior with respect to the recharge time of surface states located near the Fermi level of intrinsic semiconductor. For the structure No. 1 without a graded-gap layer, the concentration determined by the proposed method is considerably less than that determined from the value of the capacitance at the minimum of the low-frequency CV characteristic. The CV characteristics of the MIS-structure No. 1 without a graded-gap layer at a frequency of 100 kHz are not high-frequency with respect to the recharge time of surface states located near the Fermi level of intrinsic semiconductor. Dopant concentrations determined from the slope of the dependence $1/C^2(V)$ in the depletion mode are somewhat higher than the values

TABLE 2. Values of the Characteristic Capacitances and Dopant Concentrations Determined by Various Methods for the Structures Nos. 1 and 2

Number of the structure	C_{HFinv}, pF	Concentration determined by the proposed technique, cm^{-3}	C_{LFmin}, pF	Concentration determined from the minimum of the LF CV characteristic, cm^{-3}	Concentration determined from the dependence $1/C^2(V)$, cm^{-3}
1	41.27	$5.49 \cdot 10^{14}$	66.2	$1.87 \cdot 10^{15}$	$2.91 \cdot 10^{15}$
2	30.24	$1.17 \cdot 10^{15}$	30.72	$8.80 \cdot 10^{14}$	$1.91 \cdot 10^{15}$

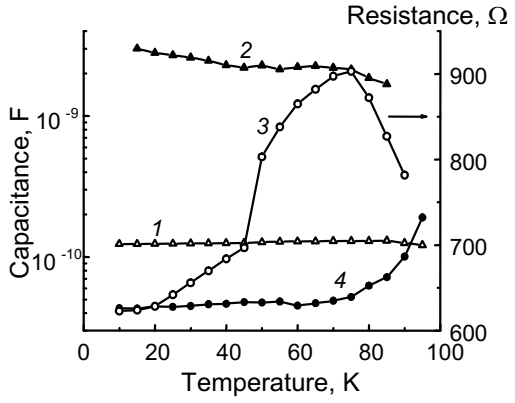

Fig. 6

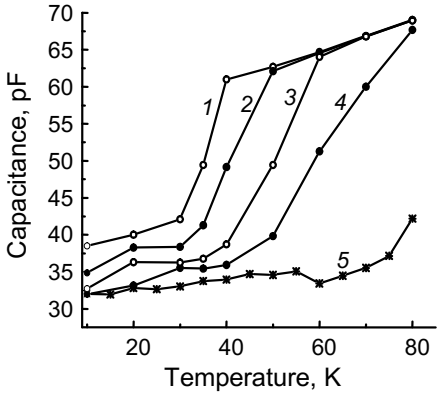

Fig. 7

Fig. 6. Temperature dependences of parameters of the equivalent circuit elements in the strong inversion mode for the MIS structure based on *n*-HgCdTe without a graded-gap layer (the structure No. 1) determined by the proposed method (f_1 = 200 kHz and f_2 = 500 kHz): *1* – C_{ins}, *2* – C_p, *3* – R_{SCR}, and *4* – C_{SCR}.

Fig. 7. Temperature dependences of the experimental capacitance values in the minimum of the CV characteristic for the MIS structure based on *n*-HgCdTe without a graded-gap layer (the structure No. 1) and the temperature dependence of the high-frequency capacitance in the strong inversion mode determined by the proposed method (*5*). Experimental dependences are measured at various frequencies, kHz: 10 (*1*), 20 (*2*), 50 (*3*), and 100 (*4*).

determined by the proposed method, which may be associated with a more weak voltage dependence of the surface potential in the real structure due to the surface state recharge under the bias voltage change. Note that the concentrations in the near-surface layer determined by the proposed method are higher than the concentration found by the Hall method. For the structure No. 1 without a graded-gap layer, the measured concentration is higher by about 20%, and for the structure No. 2 with a graded-gap layer, a more than two-fold increase in the concentration of the dopant in the near-surface layer is observed. It is difficult to say, whether this increase of the concentration is due to the type of the insulator coating, or to the presence of a graded-gap layer in the near-surface region of the semiconductor.

Let us consider the dependences of parameters of the equivalent circuit elements in the strong inversion on the temperature and bias voltage for the structure No. 1 without a graded-gap layer. Figure 6 shows the temperature dependences of the parameters of the equivalent circuit elements in the strong inversion determined by the proposed method for the structure No. 1 in the temperature range 10–80 K. As can be seen from Fig. 6, the insulator capacitance is weakly dependent on temperature, the inversion layer capacitance decreases slightly during heating from 10 to 80 K, and the SCR capacitance slowly increases upon heating at low temperatures and increases rapidly at higher temperatures. The SCR resistance is changed non-monotonically with increasing temperature. Figure 7 demonstrates the

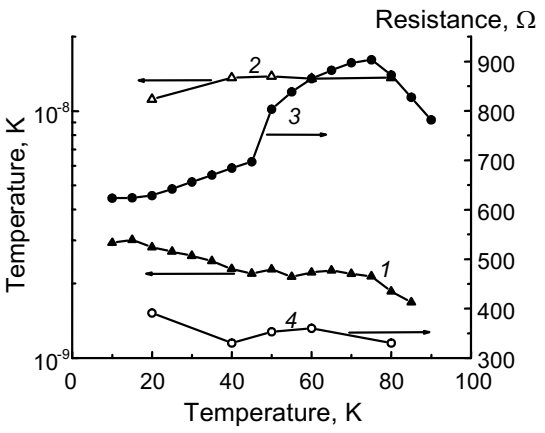

Fig. 8

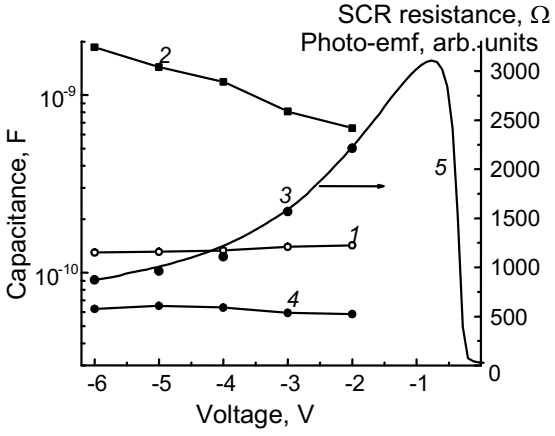

Fig. 9

Fig. 8. Temperature dependences of the inversion layer capacitance and the differential resistance of the SCR in the strong inversion in the dark (*1* and *3*) and under illumination by LED radiation (*2* and *4*) by LED radiation determined for the MIS structure based on *n*-HgCdTe without a graded-gap layer (the structure No. 1) by the proposed method (f_1 = 200 kHz and f_2 = 500 kHz): *1*, *2* – C_p, *3*, *4* – R_{SCR}.

Fig. 9. Bias dependences of parameters of the equivalent circuit elements in the strong inversion mode for the MIS structure based on *n*-HgCdTe without a graded-gap layer (the structure No. 1) determined by the proposed method at T= 80 K (f_1 = 200 kHz and f_2 = 500 kHz) and the bias dependence of the photo-emf: *1* – C_{ins}, *2* – C_p, *3* – R_{SCR}, and *4* – C_{SCR}, and *5* – photo-emf.

temperature dependences of the capacitance for the structure No. 1 in the minimum of the CV characteristics measured at different frequencies, as well as the dependence of the high-frequency capacitance in the strong inversion on temperature calculated by the proposed method. The lack of smoothness in the experimental curves is associated with a large voltage step (0.1 V) in carrying out these measurements. It can be concluded from Fig. 7 that at low temperatures, CV characteristics at frequencies of 10–100 kHz for the structure No. 1 without a graded-gap layer become high-frequency relative to the recharge time of surface states located near the Fermi level of intrinsic semiconductor. The higher the frequency, the higher the temperature, at which the CV characteristics become high-frequency with respect to the recharge time of surface states.

Figure 8 shows the temperature dependences of the inversion layer capacitance and differential resistance of the SCR in the dark mode and under illumination by the constant LED radiation (λ = 0.94 μm). It is seen from Fig. 8 that when illuminated, the capacitance of the inversion layer is increased by 3–5 times, and the SCR resistance is decreased by 2–3 times. The decrease of the SCR differential resistance under illumination is associated with the appearance of an additional source of minority charge carriers in the SCR due photogeneration. From Fig. 9, where the dependences of the equivalent circuit elements in strong inversion on the bias voltage are demonstrated, it is seen that the insulator and SCR capacitances are practically independent of the bias voltage in the strong inversion mode. The capacitance of the inversion layer is increased by the bias of the structure further in the region of strong inversion (when applying large negative voltages), and the differential resistance of the SCR is decreased, when applying large negative voltages. Curve *5* in Fig. 9 also shows the dependence of the photo-emf measured for this structure at 80 K. It is evident that the photo-emf and the differential resistance of the SCR in the strong inversion mode are decreased in a similar manner. A decrease in the photo-emf of MIS structures based on *n*-$Hg_{1-x}Cd_xTe$ (x = 0.21–0.23) in the strong inversion mode is typical for structures without a graded-gap layer and is associated with an increase in the tunneling generation current

via deep levels in the strong inversion [28]. Note that the voltage dependences (*3*) and (*5*) are similar to each other. The photo-emf value is given in arbitrary units.

We consider the expressions for the SCR capacitance and the capacitance of the inversion layer. In the calculation, the following expressions for the band gap width (E_g), intrinsic concentration (n_i), and permittivity (ε_s) in HgCdTe were used [1]:

$$E_g = -0.302 + 1.93x - 0.81x^2 + 0.832x^3 + 5.35\cdot 10^{-4}(1-2x)T,$$

$$n_i = (5.585 - 3.82x + 0.001753T - 0.001364xT)\cdot 10^{14}\cdot E_g^{1.5}T^{1.5}\exp\left(-\frac{E_g}{2kT}\right), \quad (6)$$

$$\varepsilon_s = 20.5 - 15.6x + 5.7x^2,$$

where T is the temperature and x is the content of CdTe in $Hg_{1-x}Cd_xTe$.

At a high frequency in the strong inversion, the measured capacitance C_{HFinv} is constant, has a minimal value, and is determined by the concentration of majority carriers in the near-surface region of the semiconductor, as well as by the intrinsic concentration and temperature. For the SCR capacitance, we can write the following expression [7, 24, 27]:

$$C_{SCR} = \frac{\varepsilon_s\varepsilon_0 S}{W_{max}},\ W_{max} = \sqrt{\frac{4\varepsilon_s\varepsilon_0 kT\ln\left(\frac{N_d}{n_i}\right)}{q^2 N_d}}, \quad (7)$$

where W_{max} is the maximum equilibrium width of the SCR, which is realized in the strong inversion, S is the field electrode area, k is the Boltzmann constant, and q is the electron charge.

Figure 10 shows the calculation results of the temperature dependences of the SCR capacitance at the electron concentration $5.49\cdot 10^{14}$ cm^{-3} and the dependence constructed by the proposed method. Figure 10 demonstrates that there is qualitative agreement between the calculated curve and the dependence constructed using experimental data. The high-temperature rise is associated with the increase in the intrinsic charge carrier concentration.

The temperature dependence of the inversion capacitance was calculated within the framework of various approximations. The equilibrium concentrations of electrons and holes can be written as follows taking into account the Fermi–Dirac distribution:

$$n_0 = n_i F_{0.5}(\eta_{f,c}) / F_{0.5}(\eta_{i,c}),$$

$$p_0 = n_i F_{0.5}(\eta_{v,f}) / F_{0.5}(\eta_{v,i}),$$

where $\eta_{ab} = (E_a - E_b)/kT$ is the dimensionless parameter of the energy value, E_f is the Fermi level energy in the semiconductor, E_c is the energy of the conduction band bottom, E_v is the energy of the valence band top, E_i is the Fermi level energy of an intrinsic semiconductor, and $F_{0.5}(\eta_{ab})$ is the Fermi-Dirac integral [3] with $j = 0.5$:

$$F_j(\eta_{ab}) = \int_0^\infty \frac{x^j dx}{1+\exp(x-\eta_{ab})} n_i\ .$$

The expression for the capacitance of holes in the strong inversion mode for MIS structures based on *n*-HgCdTe has the following form [3]:

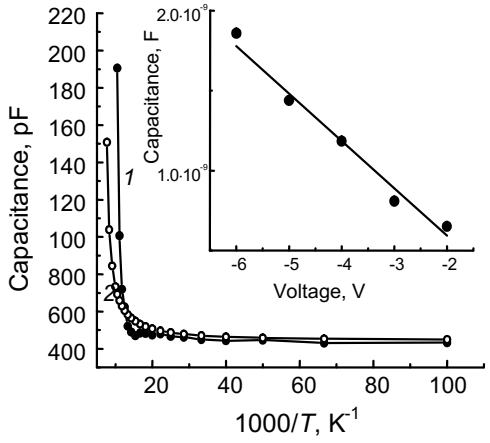

Fig. 10. Dependences of the SCR capacitance in the strong inversion on the reciprocal temperature for the MIS structure based on *n*-HgCdTe without a graded-gap layer (the structure No. 1): *1* – the capacitance is determined by the proposed method (f_1 = 200 kHz and f_2 = 500 kHz), *2* – the calculation. In the inset – the dependence of the inversion capacitance on the bias voltage (points) and the calculated dependence (line).

$$C_p(y_s) = \mathrm{sign}(y_s)\frac{\varepsilon_s\varepsilon_0}{4L_D}\frac{H(y_s)}{\sqrt{G(y_s)}}, \tag{8}$$

where L_D is the screening length for the intrinsic semiconductor, equal to

$$L_D = \sqrt{\frac{kT\varepsilon_s\varepsilon_0}{q^2 n_i}},$$

$G(y_s)$ and $H(y_s)$ are the functions defined as follows:

$$H(y_s) = \frac{F_{0.5}(\eta_{v,f}) - F_{0.5}(\eta_{v,f} - y_s)}{F_{0.5}(\eta_{v,f})},\ G = -\frac{\frac{2}{3}\left(F_{1.5}(\eta_{v,f}) - F_{1.5}(\eta_{v,f} - y_s)\right) - F_{0.5}(\eta_{v,f})y_s}{F_{0.5}(\eta_{v,f})}. \tag{9}$$

The band gap width of $Hg_{0.775}Cd_{0.225}Te$ at 77 K is 0.123 eV. The energy position of the Fermi level of the intrinsic semiconductor HgCdTe is shifted to the conduction band by a value of [3]

$$\frac{E_g}{2} - (E_c - E_i) = \frac{4}{3}kT\ln\left(\frac{m_n}{m_p}\right), \tag{10}$$

for HgCdTe, $m_n^* \cong 0.007m_0$ and $m_p^* \cong 0.55m_0$ [3].

The inversion layer capacitance with allowance for the Maxwell-Boltzmann distribution can be written as follows:

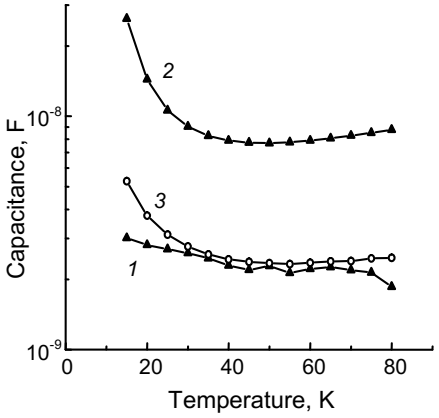

Fig. 11. Temperature dependences of the inversion layer capacitance for the MIS structure based on *n*-HgCdTe without a graded-gap layer (the structure No. 1): *1* – the capacitance is determined by the proposed method (f_1 = 200 kHz and f_2 = 500 kHz), *2* – calculation excluding the effect of the degeneracy, *3* – calculation taking into account the effect of the degeneracy.

$$C_p = \frac{\varepsilon_s \varepsilon_0}{\sqrt{2} L_{Dp}} \exp\left[-\frac{q\varphi_s}{2kT} \right], \tag{11}$$

where L_{Dp} is the screening length for holes defined by the expression

$$L_{Dp} = \sqrt{\frac{kT\varepsilon_s\varepsilon_0}{q^2 p_0}},$$

and the dimensionless surface potential (y_s) is connected with the surface potential (φ_s) (in volts) by the following relation: $y_s = \frac{q}{kT}\varphi_s$.

The dependence of the inversion capacitance on the bias voltage in the strong inversion mode can be easily constructed taking into account the Maxwell-Boltzmann distribution by using the following expression for the surface potential [24]:

$$\varphi_s = \frac{2kT}{q}\left[\ln(V) - \ln\left(\frac{kT\varepsilon_s\varepsilon_0 S}{qL_D C_{ins}} \sqrt{\frac{p_0}{n_i}} \right) \right], \tag{12}$$

where V is the bias voltage.

The points in the inset in Fig. 10 show the bias dependence of the inversion capacitance determined by means of the proposed method, and the line shows the normalized dependence calculated according to the formulas (11) and (12). It can be seen that the calculated and experimentally determined inversion capacitances increase linearly with the bias of the structure in the region of strong inversion.

Figure 11 shows the temperature dependence of the inversion capacitance constructed by the proposed method and the calculated temperature dependences at the surface potential of 0.11eV. Note that the strong inversion mode occurs when the surface potential is equal to –0.062 V.

Curve *2* in Fig. 11 is calculated by formula (11) excluding the effects of degeneracy for the Maxwell-Boltzmann distribution. Curve *3* is calculated by formulas (8) and (9) taking into account the degeneracy, the Fermi-Dirac distribution, and the temperature dependence of the Fermi level position and the Fermi level (formula (10)) for the intrinsic semiconductor. It is evident from Fig. 11 that for any calculation model, there is a fairly wide range of temperatures where the inversion capacitance depends only weakly on temperature.

CONCLUSIONS

Thus, in the temperature range of 10–100 K, admittance of MIS structures based on MBE *n*-$Hg_{0.775}Cd_{0.225}Te$ is studied in the strong inversion mode. A technique is proposed for the determining the values of parameters of the equivalent circuit elements in the strong inversion mode based on the numerical solution of a system of four equations, in which the capacitance and differential conductance values, measured at two intermediate frequencies, are used as the parameters. At a temperature of 77 K, the values of the SCR capacitance, capacitance of the inversion layer, insulator capacitance, and differential resistance of the SCR are determined for the MIS structure based on a system *n*-$Hg_{0.775}Cd_{0.225}Te/Al_2O_3$ without a near-surface graded-gap layer with high content of CdTe, as well as for the MIS structure on the basis of the system *n*-$Hg_{0.775}Cd_{0.225}Te/SiO_2/Si_3N_4$ with a graded-gap layer.

The differential resistance of the SCR in the strong inversion mode was significantly greater for the MIS structure based on *n*-$Hg_{0.775}Cd_{0.225}Te$ with a graded-gap layer, and the capacitance of the inversion layer was approximately 2 times greater for the structure without a graded-gap layer. The inversion capacitance values were quite small (of an order of $(2–3)\cdot10^{-9}$ F for the electrode area of $1.8\cdot10^{-7}$ m^2) which can be due to the effect of degeneracy in the valence band, as well as to a more flat voltage dependence of the surface potential, as compared with that in an ideal structure.

The determined values of the insulator and SCR capacitances were used to find a value of the high-frequency capacitance of the MIS structure in the inversion mode, which allowed, as a result of numerical simulation of CV characteristic, to find the majority charge carrier concentration (electrons) in the near-surface layer of the semiconductor. For the MIS structure based on *n*-$Hg_{0.775}Cd_{0.225}Te$ without a graded-gap layer, the electron concentration in the near-surface layer was sufficiently close to an integral value determined by the Hall method. For the MIS structure based on *n*-$Hg_{0.775}Cd_{0.225}Te$ with a graded-gap layer, the electron concentration in the near-surface layer exceeds the integral "Hall" value by more than 2 times. It is not established yet, whether the increase of the electron concentration in the near-surface layer is due to the presence of a graded-gap layer or to the type of the insulator coating. Note that surface treatment (including deposition of a SiO_2/Si_3N_4 insulator) may well change the electrical parameters of the near-surface layer of HgCdTe. For example, in [29], a change in the integral electrical characteristics (the concentration and mobility of majority carriers) of MBE *p*-HgCdTe heteroepitaxial films was revealed after the treatment of the film surface by polishing etchant. According to our research, in the near-surface layer of *n*-HgCdTe passivated by a double-layer SiO_2/Si_3N_4 insulator, electron concentration is greater than the average one defined by the Hall method, whereas for *p*-HgCdTe with a SiO_2/Si_3N_4 insulator, hole concentration is less than average "Hall" concentration of holes, if it is not higher than 10^{16} cm^{-3}. It can be assumed that deposition of a double-layer SiO_2/Si_3N_4 insulator leads to some decrease in the concentration of mercury vacancies, which are the defects of acceptor type. In addition, for an electronic material, the difference $N_d–N_a$ is increased resulting in an increase in the electron concentration in the near-surface region [30]. It is shown that the CV characteristics of the structure with a graded-gap layer at a frequency of 100 kHz, have high-frequency behavior with respect to the recharge time of surface states located near the Fermi level of intrinsic semiconductor. For the structure without a graded-gap layer at a frequency of 100 kHz, the CV characteristics have no high-frequency behavior with respect to the recharge time of surface states located near the Fermi level of intrinsic semiconductor. It should be noted that at decreasing temperature down to 10 K, the CV characteristics for the structure without a graded-gap layer also become high-frequency relative to the recharge time of surface states.

For the MIS-structure based on *n*-$Hg_{0.775}Cd_{0.225}Te$ without a graded-gap layer, the temperature and voltage dependences of the parameters of main equivalent circuit elements are studied in the strong inversion mode (the SCR capacitance, the capacitance of the inversion layer, the insulator capacitance, and the differential resistance of the SCR).

The insulator capacitance is practically independent of the temperature and voltage, which indicates a weak temperature dependence of the permittivity in the temperature range 10–100 K. The SCR capacitance increases significantly in the temperature range of 80-100 K, where the contribution of intrinsic concentration to the total concentration of majority charge carriers cannot be neglected. The capacitance of the inversion layer is reduced by about 40% when heated from 10 to 80 K. The resistance of the SCR is non-monotonic and varies slightly with increasing temperature from 10 to 90 K. At a temperature of about 75 K, a high-temperature decrease of the differential resistance of the SCR starts, which is related to the diffusion of minority carriers from a quasi-neutral bulk to the surface. The diffusion flux increases with an increase in the intrinsic concentration associated with an increase in temperature. In the temperature range of 10–75 K, the differential resistance of the SCR is limited by the tunneling processes via deep levels, as confirmed by an independent measurement of the photo-emf dependence on the bias voltage. Illumination by a constant LED radiation through the substrate practically does not change the temperature dependences of the insulator and SCR capacitances, but it leads to a decrease of the differential resistance of the SCR due to the appearance of an additional source of minority carriers in the SCR caused by photogeneration, as well as to a 3–5-fold increase in the inversion layer capacitance. Somewhat unusual appears that by increasing the capacitance of the inversion layer, no appreciable increase in the capacitance measured in the strong inversion occurs. With an increase in the absolute value of the negative voltage, biasing the structure in the strong inversion, an increase in the inversion layer capacitance and a decrease in the differential resistance of the SCR are observed. It is shown that the decrease of the differential resistance of the SCR, if the structure is biased in the strong inversion, practically coincides with the decrease of the normalized photo-emf, which agrees well with traditional ideas about the formation of the photo-emf in MIS structures [3]. The results obtained are in good agreement with the temperature and voltage dependences of the inversion capacitance and SCR resistance previously studied for MIS structures based on MBE *p*-$Hg_{1-x}Cd_xTe$ (x = 0.22–0.23) [16]. The results of calculation of the temperature and voltage dependences of parameters of the equivalent circuit elements are qualitatively consistent with the dependences constructed on the basis of the admittance measurements.

The work was financially supported by the Russian Foundation for Basic Research and the Administration of Tomsk region as part of a Research Project No. 16-42-700759. This work was supported in part by the Grant (No. 8.2.10.2015) within the “The Tomsk State University Academic D. I. Mendeleev Fund Program” in 2016. The authors are grateful to the staff of ISP SB RAS V. S. Varavin, V. V. Vasil’ev, S. A. Dvoretskii, N. N. Mikhailov, M. V. Yakushev, G. Yu. Sidorov, and I. O. Parm for providing the MBE HgCdTe samples.

REFERENCES

1. A. Rogal’skii, Infrared Detectors/ed. A. V. Voitsekhovskii [Russian translation], Nauka, Novosibirsk (2003).
2. J. Chu and A. Sher, Device Physics of Narrow Gap Semiconductors, Springer, N. Y. (2010).
3. A. V. Voitsekhovskii and V. N. Davydov, Photovoltaic MIS-Structures of the Narrow-Gap Semiconductors [in Russian], Radio I Svyaz, Tomsk (1990).
4. N. Wang, S. Liu, T. Lan, *et al*., Proc. SPIE, **8419**, 84191D (2012).
5. G. H. Tsau, A. Sher, M. Madou, *et al*., J. Appl. Phys., **59**, No. 4, 1238–1244 (1986).
6. Y. Nemirovsky and I. Bloom, J. Vac. Sci. Technol. A, **6**, No. 4, 2710–2715 (1988).
7. E. H. Nicollian and J. R. Brews, MOS (Metal Oxide Semiconductor) Physics and Technology, Wiley, New-York (1982).
8. A. V. Voitsekhovskii, S. N. Nesmelov, and S. M. Dzyadukh, Russ. Phys. J., **52**, No. 10, 1003–1020 (2009).
9. V. N. Ovsyuk, G. L. Kuryshev, Yu. G. Sidorov, *et al*., Matrix Photodetector Devices of Infrared Region [in Russian], Nauka, Novosibirsk (2001).
10. V. N. Ovsyuk and A. V. Yartsev, Proc. SPIE, **6636**, 663617–663621 (2007).
11. V. V. Vasil’ev and Yu. P. Mashukov, Semiconductors, **41**, No. 1, 37–42 (2007).
12. D. I. Gorn, S. N. Nesmelov, A. V. Voitsekhovskii, *et al*., Izv. Vyssh. Uchebn. Zaved. Fizika, **51**, No. 9/3, 134 (2008).
13. A. V. Voitsekhovskii, S. N. Nesmelov, and S. M. Dzyadukh, Opto-Electron. Rev., **22**, No. 4, 236–244 (2014).
14. A. V. Voitsekhovskii, S. N. Nesmelov, S. M. Dzyadukh, *et al*., Russ. Phys. J., **57**, No. 4, 536–544 (2014).

15. A. V. Voitsekhovskii, S. N. Nesmelov, S. M. Dzyadukh, *et al*., Infrared Phys. Technol., **71**, 236–241 (2015).
16. A. V. Voitsekhovskii, S. N. Nesmelov, S. M. Dzyadukh, *et al*., Russ. Phys. J., **57**, No. 8, 1070–1081 (2014).
17. A. V. Voitsekhovskii, S. N. Nesmelov, and S. M. Dzyadukh, Russ. Phys. J., **58**, No. 4, 540–551 (2015).
18. M. Michael and W. F. Leonard, Solid-State Electron., **17**, 71–85 (1974).
19. I. Bloom and Y. Nemirovsky, Solid-State Electron., **31**, 17–25 (1988).
20. R. K. Bhan and V. Dhar, Semicond. Sci. Technol., **19**, 413–416 (2004).
21. Z. J. Quan, G. B. Chen, L. Z. Sun, *et al*., Infrared Phys. Technol., **50**, 1–8 (2007).
22. R. Fu and J. Pattison, Opt. Eng., **51**, No. 10, 104003(1–4) (2012).
23. V. V. Vasilyev, A. V. Voitsekhovskii, F. N. Dultsev, *et al*., Prikladn. Fiz., No. 5, 63–66 (2007).
24. V. I. Gaman, Physics of Semiconductor Devices [in Russian], Izd. NTL, Tomsk (2000).
25. A. V. Voitsekhovskii, S. N. Nesmelov, S. M. Dzyadukh, *et al*., Prikladn. Fiz., No. 5, 80–86 (2011).
26. W. Van Gelder and E. H. Nicollian, J. Electrochem. Soc., **118**, No. 1, 138–141 (1971).
27. V. M. Koleshko and G. D. Kaplan, Obz. Elektron. Tekh. Mikroelektron., No. 2(465), 82 (1977).
28. A. V. Voitsekhovskii, S. N. Nesmelov, S. M. Dzyadukh, *et al*., Russ. Phys. J., **55**, No. 8, 917–924 (2013).
29. E. V. Permikina and A. S. Kashuba, Usp. Prikladn. Fiz., **3,** No. 2, 180–189 (2015).
30. A. V. Voitsekhovskii, D. V. Grigor'ev, and N. Kh. Talipov, Russ. Phys. J., **51**, No. 10, 1001–1015 (2008).